Available online at www.sciencedirect.com
SCIENCE DIRECT®
Journal of Sound and Vibration 271 (2004) 67–81
JOURNAL OF SOUND AND VIBRATION
www.elsevier.com/locate/jsvi

Analytic trapezoidal Fourier *p*-element for vibrating plane problems

A.Y.T. Leung*, Bin Zhu, Jianjin Zheng, Hao Yang

Department of Building and Construction, City University of Hong Kong, Tatchee Avenue, HKSAR, China

Received 13 August 2002; accepted 17 February 2003

Abstract

A trapezoidal Fourier *p*-element for the in-plane vibration analysis of two-dimensional elastic solids is presented. Trigonometric functions are used as enriching functions instead of polynomials to avoid ill-conditioning problems. The element matrices are analytically integrated in closed form. With the additional Fourier degrees of freedom (d.o.f.s), the accuracy of the computed natural frequencies is greatly increased. One element can predict many modes accurately. Since a triangle can be divided into three trapezoidal elements, the range of application is much wider than the previously derived rectangular Fourier *p*-element. Numerical examples show that convergence is very fast with respect to the number of trigonometric terms. Comparison of natural modes calculated by the trapezoidal Fourier *p*-element and the conventional finite elements is carried out. The results show that the trapezoidal Fourier *p*-element produces much higher accurate modes than the conventional finite elements with the same number of d.o.f.s. For a benchmark problem, the condition number of the mass matrix using Legendre *p*-element increases rapidly and it becomes non-positive with 22 terms. The condition numbers of the Fourier *p*-element matrices are consistently much lower than those of the Legendre *p*-element.

1. Introduction

Many engineering vibration problems can be analyzed by plane stress or plane strain problems for simplicity. Isoparametric quadrilateral elements with analytic integrals for stiffness matrix and mass matrix [1–3] are widely used. Hybrid elements including assumed hybrid stress method [4–7] and assumed hybrid strain method [8,9] were developed based on the isoparametric coordinates and the internal incompatible displacements.

*Corresponding author. Tel.: +852-2788-7600; fax: +852-2788-9643.
E-mail address: andrew.leung@cityu.edu.hk (A.Y.T. Leung).

0022-460X/03/$ - see front matter
doi:10.1016/S0022-460X(03)00263-3

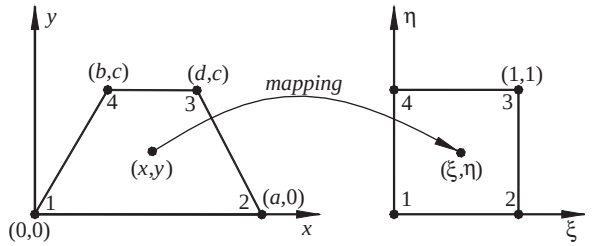

Fig. 1. The trapezoidal element co-ordinate transformation.

The accuracy of solutions using the finite element method may be improved in two ways. The first is the *h*-version to refine the finite element mesh and the second is the *p*-version to increase the order of polynomial shape functions for a fixed mesh. In general, *p* convergence is more rapid per degree of freedom (d.o.f.) [10]. Legendre polynomials were used as hierarchical shape functions to form the Legendre *p*-element to analyze plane problems [11]. In a *p*-version finite element method, the trigonometric functions are more effective in predicting the medium- and high-frequency modes than polynomials both in precision and in avoiding the ill-conditioning problems [12,13]. The Fourier *p*-version elements are popular for the dynamic problems [14,15]. Rectangular elements are good for the vibration analyses with regular shapes such as square, *L*- and *H*-shapes. For irregular polygonal shapes, triangular elements are useful. However, the existing triangular membrane Fourier *p*-element [14] cannot be integrated analytically introducing numerical integration errors. The problem becomes obvious for higher Fourier terms that are oscillating. One can always break a triangle into three trapezoids by drawing three lines parallel to the edges from any point inside the triangle. So the trapezoidal Fourier *p*-element with analytic integration can obtain very high vibration modes for the arbitrary polygons accurately. It is noted that the total number of d.o.f. of a triangle consisting of three trapezoids is greater than that of a single triangular element. Leung and Chan [16] gave the trigonometric shape functions for the axial vibration analysis of a two-node bar. The trigonometric shape functions can be extended to that for the trapezoidal Fourier *p*-element by co-ordinate transformation as shown in Fig. 1.

In order to examine the present element, some two-dimensional numerical examples are given. In a benchmark test, the matrix condition number of the Legendre *p*-element increases rapidly and the mass matrix becomes non-positive when 22 Legendre hierarchical terms were used. The matrix condition number of the Fourier *p*-element is consistently lower than those of the Legendre *p*-element and no failure was observed. The analytic trapezoidal Fourier *p*-element is indeed more effective than both the conventional finite element and the orthogonal Legendre *p*-element in predicting the medium- and high-frequency modes for the same number of degrees of freedom (d.o.f.s).

2. Formulation

2.1. Shape functions

Leung et al. [16] adopted the Fourier-enriched shape functions $f_i(\zeta) = [1-\zeta, \zeta, \sin(p\pi\zeta)]$ $(p = 1, 2, \ldots)$ to analyze the axial vibration of a two-node bar. The sine functions represent

internal d.o.f.s. The shape functions can be easily extended to that for analyzing two-dimensional problems:

$$N_i(\xi,\eta)=\sum_{k=1}^{p+2}\sum_{l=1}^{q+2} f_k(\xi)f_l(\eta),\quad i=1,2,\ldots(p+2)(q+2). \tag{1}$$

The four shape functions without enriching sine functions are commonly used in the Q4 element [17]. The trigonometric shape functions lead to zero displacement at each node. The shape functions with one sine series enrich the flexibility along the edges and the shape functions using double sine series give additional freedom to the interior of the element.

2.2. Stiffness matrix and mass matrix

The co-ordinate systems used to define a trapezoidal plane element are shown in Fig. 1. It is mapped into a square region in the $\xi-\eta$ plane, and the Cartesian co-ordinates x and y can be defined by

$$x=[(1-\xi)(1-\eta),\xi(1-\eta),\xi\eta,(1-\xi)\eta]\cdot[x_1,x_2,x_3,x_4]^{\mathrm{T}}, \tag{2a}$$

$$y=[(1-\xi)(1-\eta),\xi(1-\eta),\xi\eta,(1-\xi)\eta]\cdot[y_1,y_2,y_3,y_4]^{\mathrm{T}}, \tag{2b}$$

where x_i and y_i are the values of Cartesian co-ordinates at the four corner nodes, respectively. The Jacobian matrix is defined in terms of the Cartesian co-ordinates at the four corner nodes:

$$\mathbf{J}=\begin{bmatrix}\dfrac{\partial x}{\partial\xi} & \dfrac{\partial y}{\partial\xi}\\ \dfrac{\partial x}{\partial\eta} & \dfrac{\partial y}{\partial\eta}\end{bmatrix}=\begin{bmatrix}a+e\eta & 0\\ b+e\xi & c\end{bmatrix}, \tag{3}$$

where $e=d-b-a$. Then the determinant of Jacobian is $|J|=c(a+e\eta)$, and

$$\mathbf{J}^{-1}=\begin{bmatrix}\dfrac{1}{|J|} & 0\\ -\dfrac{b+e\xi}{c|J|} & \dfrac{1}{c}\end{bmatrix}=\begin{bmatrix}\bar{J}_{11} & \bar{J}_{12}\\ \bar{J}_{21} & \bar{J}_{22}\end{bmatrix}. \tag{4}$$

The displacement functions can be expressed as

$$\begin{Bmatrix}u\\ v\end{Bmatrix}=\begin{bmatrix}N_1 & 0 & N_2 & 0 & N_i & 0 & \cdots\\ 0 & N_1 & 0 & N_2 & 0 & N_i & \cdots\end{bmatrix}\boldsymbol{\delta}^e,\quad i=3\sim(p+2)(q+2), \tag{5}$$

where $\boldsymbol{\delta}^e$ is the vector of nodal displacement. Substituting Eq. (5) into the strain equations gives

$$\boldsymbol{\varepsilon} = \begin{Bmatrix} \dfrac{\partial u}{\partial x} \\ \dfrac{\partial v}{\partial y} \\ \dfrac{\partial u}{\partial y} + \dfrac{\partial v}{\partial x} \end{Bmatrix} = \begin{bmatrix} \bar{J}_{11} & \bar{J}_{12} & 0 & 0 \\ 0 & 0 & \bar{J}_{21} & \bar{J}_{22} \\ \bar{J}_{21} & \bar{J}_{22} & \bar{J}_{11} & \bar{J}_{12} \end{bmatrix} \begin{Bmatrix} \dfrac{\partial u}{\partial \xi} \\ \dfrac{\partial u}{\partial \eta} \\ \dfrac{\partial v}{\partial \xi} \\ \dfrac{\partial v}{\partial \eta} \end{Bmatrix} = \mathbf{B} \cdot \boldsymbol{\delta}^e. \tag{6}$$

For the harmonic vibration of the plane problems, the stiffness matrix and the mass matrix of the element are obtained by applying the principle of minimum potential energy and the Hamilton's principle, respectively,

$$\mathbf{K}^e = \int_V \mathbf{B}^{\mathrm{T}}\mathbf{D}\mathbf{B}\,\mathrm{d}V = t \cdot \int_0^1 \int_0^1 \mathbf{B}^{\mathrm{T}}\mathbf{D}\mathbf{B} \cdot |J|\,\mathrm{d}\xi\,\mathrm{d}\eta, \tag{7}$$

$$\mathbf{M}^e = \int_V \rho\mathbf{N}^{\mathrm{T}}\mathbf{N}\,\mathrm{d}V = \rho t \cdot \int_0^1 \int_0^1 \mathbf{N}^{\mathrm{T}}\mathbf{N} \cdot |J|\,\mathrm{d}\xi\,\mathrm{d}\eta. \tag{8}$$

For a plane stress problem, the rigidity matrix is

$$\mathbf{D} = D_0 \cdot \begin{bmatrix} 1 & v & 0 \\ v & 1 & 0 \\ 0 & 0 & (1-v)/2 \end{bmatrix}, \tag{9}$$

where $D_0 = E/(1-v^2)$ with E is the Young's modulus, ρ is the density, t is the thickness of the element and v is the Possion's ratio. For the plane strain problem, E and v are substituted by $E/(1-v^2)$ and $v/(1-v)$ respectively. Since the determinant of Jacobian $|J|$ is only related to η, ξ and η can be integrated independently, so the coefficients of the stiffness matrix and the mass matrix can be given by:

if $m = 2(j + (i-1)(q+2)) - 1$ and $n = 2(l + (k-1)(q+2)) - 1$,

$$K_{m,n} = D_0 t \left\{ A^{0,0}_{(1)j,l} \cdot \left[c \cdot B^{1,1}_{(1)i,k} + \frac{1}{2c}(1-v) \cdot B^{1,1}_{(3)i,k} \right] + A^{0,1}_{(2)j,l} \cdot \left[-\frac{1}{2c}(1-v) \cdot B^{1,0}_{(2)i,k} \right] + A^{1,0}_{(2)j,l} \cdot \left[-\frac{1}{2c}(1-v) \cdot B^{0,1}_{(2)i,k} \right] + A^{1,1}_{(3)j,l} \cdot \left[\frac{1}{2c}(1-v) \cdot B^{0,0}_{(1)i,k} \right] \right\}; \tag{10a}$$

else if $m = 2(j + (i-1)(q+2)) - 1$ and $n = 2(l + (k-1)(q+2))$,

$$K_{m,n} = D_0 t \left\{ A^{0,0}_{(1)j,l} \cdot \left[-\frac{1}{2}(1+v) \cdot B^{1,1}_{(2)i,k} \right] + A^{0,1}_{(2)j,l} \cdot [v \cdot B^{1,0}_{(1)i,k}] + A^{1,0}_{(2)j,l} \cdot \left[\frac{1}{2}(1-v) \cdot B^{0,1}_{(1)i,k} \right] \right\}; \tag{10b}$$

else if $m = 2(j + (i-1)(q+2))$ and $n = 2(l + (k-1)(q+2)) - 1$,

$$K_{m,n} = D_0 t\left\{ A^{0,0}_{(1)j,l} \cdot \left[-\frac{1}{2}(1+\nu) \cdot B^{1,1}_{(2)i,k} \right] + A^{1,0}_{(2)j,l} \cdot [\nu \cdot B^{0,1}_{(1)i,k}] + A^{0,1}_{(2)j,l} \cdot \left[\frac{1}{2}(1-\nu) \cdot B^{1,0}_{(1)i,k} \right] \right\}; \quad (10c)$$

else if $m = 2(j + (i-1)(q+2))$ and $n = 2(l + (k-1)(q+2))$,

$$K_{m,n} = D_0 t\left\{ A^{0,0}_{(1)j,l} \cdot \left[\frac{1}{c} \cdot B^{1,1}_{(3)i,k} + \frac{c}{2}(1-\nu) \cdot B^{1,1}_{(1)i,k} \right] + A^{0,1}_{(2)j,l} \cdot \left[-\frac{1}{c} \cdot B^{1,0}_{(2)i,k} \right] + A^{1,0}_{(2)j,l} \cdot \left[-\frac{1}{c} \cdot B^{0,1}_{(2)i,k} \right] + A^{1,1}_{(3)j,l} \cdot \left[\frac{1}{c} \cdot B^{0,0}_{(1)i,k} \right] \right\}; \quad (10d)$$

else if $m = 2(j + (i-1)(q+2)) - 1$ and $n = 2(l + (k-1)(q+2)) - 1$, or, $m = 2(j + (i-1)(q+2))$ and $n = 2(l + (k-1)(q+2))$, that is to say, m and n are both even or odd,

$$M_{m,n} = \rho t A^{0,0}_{(2)i,k} B^{0,0}_{(1)j,l}; \quad (11a)$$

else then

$$M_{m,n} = 0. \quad (11b)$$

The integrals are

$$A^{\alpha,\beta}_{(\mu)i,k} = \int_0^1 \frac{1}{(a+e\eta)^{2-\mu}} \cdot f_i^{\alpha} f_k^{\beta} \, \mathrm{d}\eta, \quad (12a)$$

$$B^{\alpha,\beta}_{(1)i,k} = \int_0^1 f_i^{\alpha} f_k^{\beta} \, \mathrm{d}\xi, \quad (12b)$$

$$B^{\alpha,\beta}_{(2)i,k} = \int_0^1 (b+e\xi) f_i^{\alpha} f_k^{\beta} \, \mathrm{d}\xi, \quad (12c)$$

$$B^{\alpha,\beta}_{(3)i,k} = \int_0^1 (b+e\xi)^2 f_i^{\alpha} f_k^{\beta} \, \mathrm{d}\xi, \quad (12d)$$

where $i,k = 1,2,\ldots,p+2$, $j,l = 1,2,\ldots,q+2$, $\mu = 1 \sim 3$ and the superscripts α and β ($\alpha,\beta = 0,1$) denote the order of the derivatives.

For the rectangular element, $e = 0$ and $b = 0$. For the skew element, $e = 0$. There is no problem in the integrals of their coefficients of mass and stiffness matrices. For the trapezoidal plane element, the problem reduces to the integration of $\eta^k/(a+e\eta)$ and $\exp(\mathrm{i}k\pi\eta)/(a+e\eta)$. The former does not require much attention and the latter is equal to $(1/e)\exp(-\mathrm{i}k\beta\pi) \cdot (\mathrm{Ei}(-\mathrm{i}k\beta\pi) - \mathrm{Ei}(-\mathrm{i}k(1+\beta)\pi))$ where $\beta = a/e$ and Ei is the exponential integral function. The exact values of the above integrals will be easily obtained if some commercial packages such as Matlab and Maple are used.

2.3. Free vibration analysis of structures

With the above analytical integrals, the stiffness matrix and the mass matrix of the element with order $R = (p+2)(q+2)$ are rather straightforward. The stiffness matrix and the mass matrix obtained by Eqs. (10) and (11), respectively can be stored in two individual files. These files are

later used to compute the natural frequencies of the plane problems. If the integrals were evaluated numerically using Gaussian quadrature such as those of the triangular Fourier *p*-element [14], the shape functions of the element do not satisfy the requirement of completeness and numerical errors increase with the order, which is the number of Fourier terms, due to increasingly high oscillation. The Gaussian quadrature can only be used to predict several lowest frequencies with few Fourier terms. Alternatively, a triangular element can be divided into three trapezoidal elements by drawing three lines parallel to the edges from any point inside the triangle. With the analytical integral formulae (12), the stiffness matrix and mass matrix for a triangular Fourier *p*-element of any order can also be formulated for non-uniform thickness.

Before assembling the elements, the internal d.o.f.s and the d.o.f.s on some edges and at corner nodes not adjacent to other elements can be condensed by exact dynamic condensation [18]. The assembling is carried out by ensuring that the directions of the common edges are compactable between two adjacent elements. Then, for free vibrations one has,

$$\mathbf{K} \cdot \mathbf{u} - \lambda \cdot \mathbf{M} \cdot \mathbf{u} = 0, \tag{13}$$

where $\mathbf{K}$ is the global stiffness matrix of the structure, $\mathbf{M}$ is the global mass matrix of the structure, $\mathbf{u}$ is the eigenvector in terms of the master d.o.f.s of the structure, and $\lambda = \omega^2$ is the eigenvalue where ω is the natural frequency of the structure.

3. Numerical examples

To simplify the computation, the trigonometric term p is given the same value as q in this paper. The following several cases of in-plane vibration are used to examine the performance of the new trapezoidal Fourier *p*-element.

3.1. Longitudinal vibration of an elastic bar

The analytical solution for the vibration modes of general two-dimensional elastic solid problems is not available. Consider the longitudinal vibration of an elastic bar as shown in Fig. 2. It is a one-dimensional plane stress problem. It is well known that the analytic natural frequencies

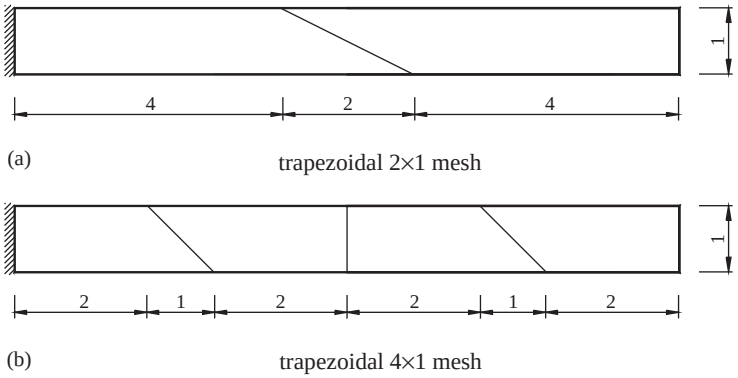

Fig. 2. Finite element model of an elastic bar.

Table 1
Values of natural frequencies for the longitudinal vibration of an elastic bar

Method		Mode 1	Mode 2	Mode 3	Mode 4	Mode 5	Mode 6	Mode 7	Mode 8
Present 2×1	$p=q=1$	0.1573	0.4856	0.9344	1.7539	2.4492	2.5102	2.6575	3.0484
	$p=q=2$	0.1572	0.4725	0.7955	1.7415	2.2382	2.2836	2.3757	2.7583
	$p=q=3$	0.1571	0.4722	0.7894	1.1079	1.4483	1.9026	2.2368	2.6649
	$p=q=4$	0.1571	0.4715	0.7869	1.1056	1.4257	1.7490	2.1129	2.4840
	$p=q=5$	0.1571	0.4714	0.7864	1.1018	1.4196	1.7418	2.0636	2.3970
	$p=q=6$	0.1571	0.4714	0.7856	1.1005	1.4158	1.7307	2.0472	2.3570
	$p=q=7$	0.1571	0.4713	0.7855	1.0999	1.4147	1.7304	2.0464	2.3570
Present 4×1	$p=q=1$	0.1571	0.4724	0.7952	1.1367	1.5706	2.0310	2.449	2.7291
	$p=q=2$	0.1571	0.4716	0.7866	1.1022	1.4207	1.7497	2.1036	2.4759
	$p=q=3$	0.1571	0.4715	0.7861	1.1018	1.4185	1.7353	2.0516	2.3703
	$p=q=4$	0.1571	0.4713	0.7856	1.1001	1.4150	1.7310	2.0485	2.3670
	$p=q=5$	0.1571	0.4713	0.7856	1.1001	1.4148	1.7297	2.0446	2.3597
	$p=q=6$	0.1571	0.4713	0.7855	1.0998	1.4142	1.7289	2.0438	2.3572
	$p=q=7$	0.1571	0.4713	0.7855	1.0998	1.4141	1.7286	2.0431	2.3568
Analytic solutions		0.1571	0.4712	0.7854	1.0996	1.4137	1.7279	2.0420	2.3562

[19] of an elastic bar with one end fixed are

$$\omega_i = \frac{(2i-1)\pi}{2L}\sqrt{\frac{E}{\rho}} \quad (i=1,2,3,\ldots), \tag{14}$$

where L is the length of the bar, E and ρ are the elastic modulus and mass per unit length of the bar. For simplicity, one takes $E=1$, $\rho=1$ and Poisson's ratio $v=0$. As shown in Fig. 2, the bar is divided into two trapezoidal element and four trapezoidal elements respectively. With increasing number of trigonometric terms p, the computed eight lowest modes are shown in Table 1 along with the analytic solutions. It is found that very fast convergence is possible with increasing number of trigonometric terms, and the present solutions with coarse mesh show high accuracy.

3.2. Free vibration of cantilever plates

The in-plane free vibration of a cantilever plate is a truly two-dimensional problem. A square cantilever plate with in-plane vibration was studied by Gupta [20] involving higher order dynamic correction terms in the associated stiffness and mass matrices and provided solutions with a 20×20 mesh of plane stress finite elements. Zhao et al. [21] gave the asymptotic solutions using four square plane stress elements. The parameters are: $E=1$, $\rho=1$ and $v=0.3$. The results computed by two trapezoidal Fourier p-elements (see Fig. 3) are compared with the solutions in Refs [20,21] together with the ones computed by Q4 elements with a fine mesh of 100×100 in Table 2. It is noted that the Gupta's solutions were computed by finite dynamic elements and they are smaller than those of Q4 elements with fine mesh. It can be found that the computed results of the present method with $p=q=6$ are in excellent agreement with those of Q4 elements.

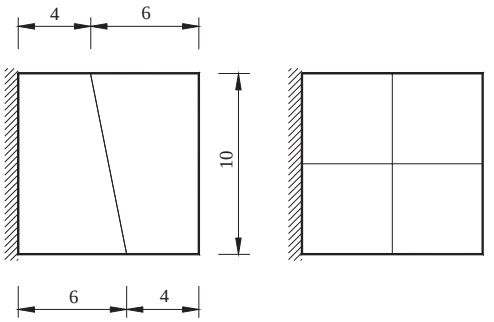

(a) trapezoidal 2×1 mesh (b) rectangular 2×2 mesh

Fig. 3. Finite element model of a square cantilever plate.

Table 2
Comparison of the natural frequencies for a square cantilever plate

Method		Mode 1	Mode 2	Mode 3	Mode 4	Mode 5	Mode 6
Present 2×1	$p = q = 1$	0.0684	0.1587	0.1840	0.3095	0.3390	0.3671
	$p = q = 2$	0.0667	0.1583	0.1791	0.2881	0.3099	0.3259
	$p = q = 3$	0.0663	0.1582	0.1785	0.2830	0.3064	0.3244
	$p = q = 4$	0.0661	0.1581	0.1778	0.2826	0.3052	0.3230
	$p = q = 5$	0.0660	0.1581	0.1777	0.2820	0.3047	0.3228
	$p = q = 6$	0.0660	0.1580	0.1775	0.2819	0.3044	0.3225
Zhao et al. [21]	Uncorrected	0.0719	0.1637	0.2090	0.3372	0.3905	0.3964
	Corrected	0.0709	0.1538	0.1899	0.2755	0.3051	0.3082
Gupta [20]	20×20	0.0659	0.1580	0.1769	0.2797	0.3034	0.3214
Q4	100×100	0.0658	0.1580	0.1772	0.2816	0.3037	0.3223

The condition number **CN** defined in Ref. [22] is used to measure the ill-conditioning in a coefficient matrix.

$$\mathbf{CN} = \frac{\lambda_{max}}{\lambda_{min}}, \tag{15}$$

where λ_{max} and λ_{min} are respectively the largest and smallest eigenvalues of the coefficient matrix. A large condition number indicates that the FEM solutions may be ill-conditioned. To study the conditioning of the Legendre p-element (or the hierarchical finite element using Legendre polynomials, HFEM) with increasing orders, the mass matrices of the square cantilever plate (see Fig. 3) using a single square mesh are computed by the Fourier p-element and HFEM whose shape functions are the same as the ones in Ref. [12]. Using the commercial package Matlab, the condition numbers of the mass matrices computed by the two methods are compared in Fig. 4. It is evident that the **CN** of the Fourier p-element is much smaller than that of HFEM. For

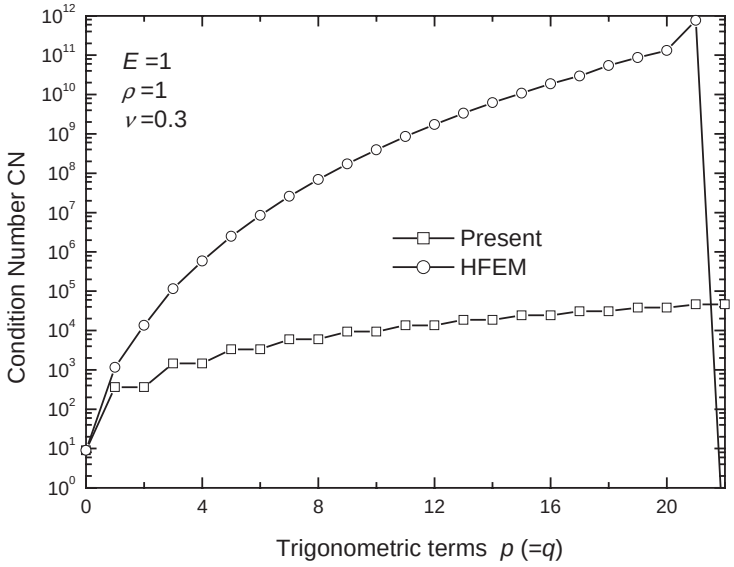

Fig. 4. Comparison of the condition number **CN** of the mass matrices between the present method and HFEM for a square cantilever plate.

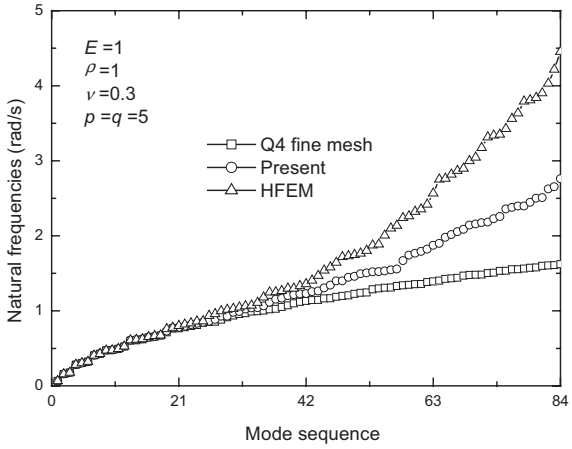

Fig. 5. Comparison of the natural frequencies between the present method and HFEM for a square cantilever plate.

$p = q = 22$, λ_{min} and the condition number of the mass matrix computed by HFEM are negative. The mass matrices of HFEM are no longer numerically positive definitive and HFEM fails to predict the natural frequencies of the plate for $p = q \geqslant 22$. The mass matrices consist of the integrals $A^{0,0}_{(2)i,k}$ and $B^{0,0}_{(1)j,l}$ which are also involved in the coefficients of the stiffness matrices. Therefore, the stiffness matrices computed by HFEM are also ill-conditioned. On the other hand, the Fourier p-element behaves well for very large orders.

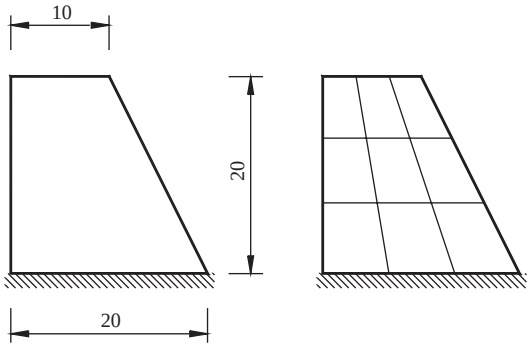

(a) trapezoidal 1×1 mesh (b) Q4 3×3 mesh

Fig. 6. Finite element model of a trapezoid cantilever plate.

Table 3
Comparison of the natural frequencies for a trapezoidal plate between the trapezoidal Fourier p-element and the four nodes isoparametric elements with the number of d.o.f.s in parentheses

Method (d.o.f.s)	Mode 1	Mode 2	Mode 3	Mode 4	Mode 5	Mode 6	Mode 7	Mode 8
$p = q = 1$(12)	0.0387	0.0879	0.1113	0.2211	0.2463	0.2808	0.3052	0.3421
Q4 2×2(12)	0.0406	0.0897	0.1277	0.2248	0.2567	0.2948	0.3090	0.3497
$p = q = 2$(24)	0.0377	0.0865	0.1003	0.1852	0.2129	0.2215	0.2483	0.2732
Q4 3×3(24)	0.0390	0.0880	0.1137	0.2055	0.2364	0.2472	0.2707	0.2957
$p = q = 3$(40)	0.0375	0.0864	0.0988	0.1779	0.2034	0.2142	0.2365	0.2588
Q4 4×4(40)	0.0380	0.0870	0.1040	0.1905	0.2173	0.2239	0.2505	0.2736
$p = q = 4$(60)	0.0374	0.0863	0.0983	0.1767	0.2012	0.2123	0.2327	0.2554
Q4 5×5(60)	0.0380	0.0870	0.1040	0.1905	0.2173	0.2239	0.2505	0.2736
$p = q = 5$(84)	0.0374	0.0863	0.0981	0.1762	0.2006	0.2118	0.2319	0.2544
Q4 6×6(84)	0.0378	0.0867	0.1022	0.1868	0.2120	0.2204	0.2456	0.2686
Q4 100×100	0.0373	0.0862	0.0977	0.1755	0.1998	0.2112	0.2304	0.2531

The natural frequencies of the plate with a single square element computed by the Fourier p-element and HFEM with $p = q = 5$ respectively are compared in Fig. 5 along with the solutions of Q4 elements with 100×100 mesh. The Fourier p-element using trigonometric shape functions is indeed more effective in predicting the medium- and high-frequency modes than the element using orthogonal Legendre polynomials as the shape functions.

With the same $2(2 + 3p + p^2)$ d.o.f.s, a trapezoidal plate with $E = 1$, $\rho = 1$ and $v = 0.3$ is taken as a trapezoidal Fourier p-element and descretized into $(p + 1)^2$ Q4 elements respectively as shown in Fig. 6. The comparison of the natural frequencies computed is carried out in Table 3 along with

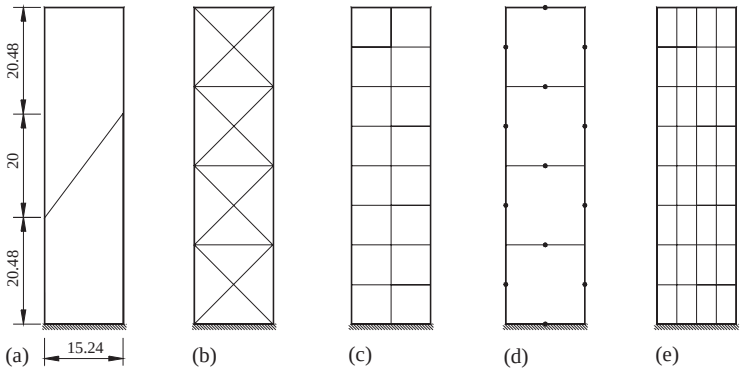

a. trapezoidal mesh
b. linear triangular mesh
c. linear rectangular mesh
d. rectangular 8-node mesh
e. RQ6 mesh

Fig. 7. Meshes of a cantilever shear wall.

Table 4
Comparison of the natural frequencies for a cantilever shear wall

Method		Mode 1	Mode 2	Mode 3[a]	Mode 4	Mode 5[a]
Analytic solution		31.247	165.820	200.710	389.972	602.130
Linear triangular		40.162	202.363	201.125	470.252	608.841
Linear rectangular		32.987	175.873	201.163	424.228	611.040
Rectangular 8-node		31.328	165.417	200.836	393.629	602.903
RQ6		31.278	164.513	—	386.994	—
Present	$p = q = 1$	33.665	200.856	202.163	517.813	624.634
	$p = q = 2$	31.940	167.888	200.836	403.067	603.178
	$p = q = 3$	31.358	164.575	200.747	381.013	602.824
	$p = q = 4$	31.270	162.309	200.730	377.590	602.047
	$p = q = 5$	31.182	161.812	200.716	375.388	601.993

[a] Modes of longitudinal vibration.

those of Q4 elements with a 100×100 mesh. It is found that the solutions using trapezoidal Fourier p-elements are more accurate than those of the Q4 elements per number of d.o.f.s. The accuracy of the solutions computed by the linear Q4 finite elements with 84 d.o.f.s (6×6) is achieved by the trapezoidal Fourier p-element method using only 24 d.o.f.s ($p = q = 2$).

A cantilever shear wall is shown in Fig. 7. Petyt [23] analyzed its first five natural frequencies using different kinds of elements and meshes as shown in Fig. 7. And then, Cheung et al. [24] applied a refined non-conforming quadrilateral element RQ6 to compute its first three natural frequencies for the flexural modes. The parameters of the shear wall are $E = 3.4474 \times 10^{10}\,\mathrm{N/m^2}$, $\rho = 568.7\,\mathrm{kg/m^3}$ and $v = 0.11$. The natural frequencies of the present element are computed and compared with those of the other elements in Table 4. The analytical solutions are obtained by

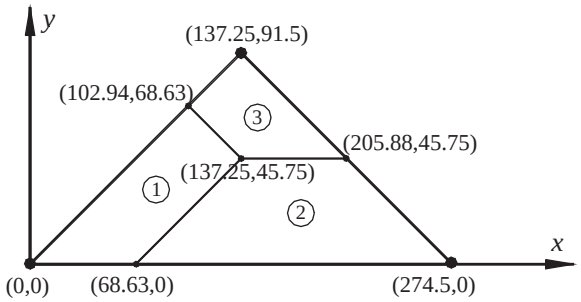

Fig. 8. Trapezoidal mesh division of an earth dam with triangular cross-section.

Table 5
Comparison of the natural frequencies for an earth dam

Mode	CST [22]	RQ6 [21]	Present				
			$p=q=1$	$p=q=2$	$p=q=3$	$p=q=4$	$p=q=5$
1	7.71	7.79	7.79	7.78	7.77	7.76	7.76
2	12.52	12.52	14.88	12.94	12.63	12.54	12.51
3	14.60	14.49	17.73	16.47	14.97	14.59	14.51
4	19.31	18.36	22.90	20.76	18.74	18.49	18.42

treating the wall as a deep beam [25]. The computed results show that the Fourier p-element can obtain the very accurate results with a simple mesh and a few trigonometric terms.

3.3. Free vibration of an earth dam

The final example is the vibration analysis of an earth dam of triangular cross-section with $E = 5.602 \times 10^8\,\mathrm{N/m^2}$, $\rho = 2080\,\mathrm{kg/m^3}$ and $v = 0.45$. This plane strain problem is derived from the plane stress problem by replacing E by $E/(1-v^2)$ and v by $v/(1-v)$. The cross-section is a triangle that can be divided into three trapezoidal Fourier p-elements as shown in Fig. 8. Clough et al. [26] analyzed this problem with 100 CST elements and 110 d.o.f.s, and then Cheung et al. [24] used 35 refined non-conforming elements with 72 d.o.f.s to obtain its first four frequencies. Their calculating results along with those of the present trapezoidal Fourier p-element are shown in Table 5. It is noted that there is little difference in the results and the maximum number of d.o.f.s is 25 in the Fourier p-element solutions, cf. 110 in Ref. [26] and 72 in Ref. [24].

4. Conclusions

A trapezoidal Fourier p-element for the vibration analysis of two-dimensional elastic solids is presented. With the analytic integration formulae, the analysis using this element is more accurate than that by using similar elements involving Gaussian quadrature. For in-plane vibration problems with shapes that must be analyzed by triangular elements, the present trapezoidal

Fourier p-element is a better choice to obtain solutions with high accuracy. The present element is indeed more effective in predicting the medium- and high-frequency modes than the element using orthogonal Legendre polynomials as shape functions both in precision and in avoiding the ill-conditioning problems.

The eight lowest modes of an elastic bar with longitudinal vibration were analyzed with different number of Fourier terms. The computed results were in good agreement with the analytic solutions using seven Fourier terms. For the in-plane vibrations of cantilever plates, comparison with the results computed by the trapezoidal Fourier p-elements and the traditional finite elements respectively was carried out to examine the effectiveness. The results showed that the trapezoidal Fourier p-element was more accurate in predicting the natural modes than the traditional finite elements per d.o.f. A triangular element could be easily divided into three trapezoidal elements by drawing three lines parallel to the edges from any point inside the triangle. In this way, an earth dam with triangular cross-section was analyzed by the present trapezoidal Fourier p-elements and the results were compared with those of previously derived elements.

Acknowledgements

The research is supported by the Hong Kong Research Grant Council of Grant #CityU 1009/02E.

Appendix A. Nomenclature

a	value of x co-ordinate at the second corner node
b	value of x co-ordinate at the fourth corner node
c	value of y co-ordinate at the third and fourth corner nodes
d	value of x co-ordinate at the third corner node
e	$=d-b-a$
N_i	element shape functions
J	Jacobian matrix
$\|J\|$	determinant of Jacobian
E	Young's modulus
ρ	mass per unit area
v	Poisson's ratio
t	uniform thickness of the element
D_0	flexural rigidity ($=E/(1-v^2)$)
x, y	Cartesian co-ordinates
ξ, η	co-ordinates in mapped plane
x_i, y_i	values of x and y co-ordinates at the four corner nodes
$\mathbf{K}^e, \mathbf{M}^e$	stiffness matrix and mass matrix of the element
K_m, M_n	coefficients of the stiffness matrix and mass matrix
$\mathbf{K}, \mathbf{M}$	stiffness matrix and mass matrix of the structure
p, q	numbers of trigonometric terms

R order of element stiffness and mass matrices
$\mathbf{u}$ eigenvector of the structure
λ eigenvalues of the structure
ω natural frequencies

References

[1] D.V. Griffiths, G.G.W. Mustoe, Selective reduced integration of four-node plane element in closed form, Journal of Engineering Mechanics 121 (1995) 725–729.
[2] L. Videla, M. Cerrolaza, N. Aparicio, Explicit integration of the stiffness matrix of a four-noded plane elasticity finite element, Communications in Numerical Methods in Engineering 12 (1996) 731–743.
[3] K.E. Barrett, Explicit eight-noded quadrilateral elements, Finite Elements in Analysis and Design 31 (1999) 209–222.
[4] T.H.H. Pian, Derivation of element stiffness matrices by assumed stress distributions, American Institute of Aeronautics and Astronautics Journal 2 (1964) 1333–1336.
[5] Y.K. Cheung, W. Chen, Refined hybrid method for plane isoparametric element using an orthogonal approach, Computers and Structures 42 (1992) 638–694.
[6] W. Chen, Y.K. Cheung, A robust refined quadrilateral plane element, International Journal for Numerical Methods in Engineering 38 (1995) 649–666.
[7] S.T. Yeo, B.G. Lee, New stress assumption for hybrid stress elements and refined four-node plane and eight-node brick elements, International Journal for Numerical Methods in Engineering 40 (1997) 2933–2952.
[8] T.J.R. Hughes, Generalization of selective integration procedures to anisotropic and nonlinear media, International Journal for Numerical Methods in Engineering 15 (1980) 1413–1418.
[9] J.C. Simo, M.S. Rifai, A class of mixed assumed strain methods and the method of incompatible medes, International Journal for Numerical Methods in Engineering 29 (1990) 1595–1638.
[10] O.C. Zienkiewicz, R.L. Taylor, The Finite Method, Vol. 1, 4th Edition, McGraw-Hill, New York, 1989.
[11] Q. Nie, Q. Niu, *p*-Version large strain finite element formulation and application in elastic–plastic deformation, Computers and Structures 65 (1997) 761–765.
[12] A. Houmat, Hierarchical finite element analysis of the vibration of membranes, Journal of Sound and Vibration 201 (1997) 465–472.
[13] N.S. Bardell, J.N. Dunsdon, R.S. Langley, Free vibration of coplanar sandwich panels, Composite Structures 38 (1997) 463–475.
[14] A. Houmat, A triangular Fourier *p*-element for the analysis of membrane vibrations, Journal of Sound and Vibration 230 (2000) 31–43.
[15] A. Houmat, A sector Fourier *p*-element for free vibration analysis of sectorial membranes, Computers and Structures 79 (2001) 1147–1152.
[16] A.Y.T. Leung, J.K.W. Chan, Fourier *p*-element for the analysis of beams and plates, Journal of Sound and Vibration 212 (1998) 179–185.
[17] R.D. Cook, Improved two-dimensional finite element, Journal of the Structure Division American Society of Civil Engineers 100 (1974) 1851–1863.
[18] A.Y.T. Leung, Dynamic Stiffness and Substructures, Springer, London, 1993.
[19] R.W. Clough, J. Penzien, Dynamic of Structures, McGraw-Hill, New York, 1975.
[20] K.K. Gupta, Development of a finite dynamic element for free vibration analysis of two-dimensional structures, International Journal for Numerical Methods in Engineering 12 (1978) 1311–1327.
[21] C. Zhao, P. Steven, Asymptotic solutions for predicted natural frequencies of two-dimensional elastic solid vibration problems in finite element analysis, International Journal for Numerical Methods in Engineering 39 (1996) 2821–2835.
[22] R.D. Cook, D.S. Malkus, M.E. Plesha, Concepts and Applications of Finite Element Analysis, 4th Edition, Wiley, New York, 1989.

[23] M. Petyt, Introduction to Finite Element Vibration Analysis, Cambridge University Press, Cambridge, UK, 1990.
[24] Y.K. Cheung, Y.X. Zhang, W.J. Chen, A refined nonconforming plane quadrilateral element, Computers and Structures 78 (2000) 699–709.
[25] J.B. Carr, The effect of shear flexibility and rotatory inertia on the natural frequencies of uniform beams, The Aeronautical Quarterly 21 (1970) 79–90.
[26] R.W. Clough, A.K. Chopra, Earthquake stress analysis in earth dams, Journal of Engineering Mechanics American Society of Civil Engineers 93 (1966) 197–211.